

An Improved Model of Convoluted Air Springs and Simulation of an Air Spring Vibration Isolation System under the Ambient Vibration

Ligang Bai[1,2] – Xipeng Wang[1] – Hui Zhuang[1,✉] – Yuanpeng Zhang[3] – Peng Chen[1] – Jianguo Ding[1,✉✉]

[1] School of Physics, Nanjing University of Science and Technology, China
[2] China Electronics System Engineering No.2 Construction Co., Ltd., China
[3] Shanghai Waigaoqiao Power Generation Co., Ltd., China

✉ zhuangh92@163.com, ✉✉ nustdjg@163.com

Abstract *This paper presents a novel double-arc geometric analytical model to analyze the static characteristics of convoluted air springs (CAS). The model assumes that the profile of the bellows is composed of double circular arcs with different radii of curvature and considers the effects of bellows stretching deformation. Based on this model, this paper proposes a hybrid analysis method that uses the CAS geometric analytical method instead of the computationally expensive fluid-structure interaction (FSI) static analysis. Using the geometric parameters and internal pressure of the CAS under loaded equilibrium, as derived from the proposed double-arc model, an FSI simulation model of the CAS is established in Fluent for subsequent static and dynamic characteristic analysis. The feasibility of the double-arc model and the proposed analysis method is validated through static and dynamic characteristic experiments of the CAS. Furthermore, the hybrid analysis method is applied to analyze the dynamic response of an air spring vibration isolation system. A comparison with the results of the traditional full-process FSI simulation demonstrates that the proposed method improves the average computation efficiency by approximately 10.8 % while maintaining computational accuracy.*

Keywords *convoluted air springs, static characteristics, dynamic characteristics, hybrid analysis method*

Highlights

- *Developed a novel double-arc geometric analytical model for CAS.*
- *Proposed an efficient hybrid analysis method for CAS FSI simulation.*
- *Validated the accuracy of the proposed model and method through experiments and full-process FSI simulations.*
- *Applied the method to simulate an air spring vibration isolation system under ambient vibration.*

1 INTRODUCTION

Advancements in sophisticated technologies, including semiconductor manufacturing and ultra-precision machining, have made the establishment of a highly stable and low-vibration operational environment essential for maintaining equipment precision [1-4]. As a conventional vibration control measure, vibration isolation systems function by blocking direct contact between the vibration source and target equipment, thereby reducing vibrational energy transmission and suppressing external excitation [5]. Currently, commonly used vibration isolation elements in vibration isolation systems include metal rubber [6], metal springs [7], rubber [8], wire ropes [9], and air springs. Among these, air springs demonstrate outstanding performance in low-frequency vibration isolation due to their combined characteristics of low natural frequency, adjustable stiffness, and lightweight design [10]. They are widely used in vibration isolation systems for automotive suspensions [11,12], rail vehicles [13,14], and industrial equipment [15-17]. In numerical simulations of the static and dynamic characteristics of air springs, fluid-structure interaction (FSI) simulation based on the finite element method has emerged as the predominant approach [18-20]. Convoluted air springs (CAS), as a widely employed structural form of air springs, typically follow this workflow for vibration isolation performance analysis: first, inflation is carried out to the specified pressure, followed by static analysis to determine equilibrium states under equipment load, and then dynamic analysis with applied excitations. However, the computational efficiency of FSI restricts the practicality of this workflow. Therefore, optimizing the CAS vibration isolation performance analysis workflow through establishing efficient analytical models for static processes holds significant engineering practical value for the performance evaluation and optimization design of vibration isolation systems.

Numerous studies have been conducted on the static and dynamic characteristics of air springs and air spring vibration isolation systems. In the field of research on the static characteristics of air springs, existing achievements have predominantly focused on two technical approaches: FSI simulations and geometric analytical methods. FSI simulations [18,19] provide high computational accuracy, but are often associated with computational inefficiency and numerical convergence challenges. Consequently, researchers have attempted to employ geometric analytical methods [20-23] to study the relationship between the vertical static stiffness of air springs and geometric as well as thermodynamic parameters. Although more efficient, geometric analytical methods are generally based on the assumption of a single-arc bellows profile, which cannot accurately describe the non-arc shapes under actual loading conditions, thereby limiting the model's applicability. Table 1 summarizes the model descriptions from key references, along with their respective advantages and disadvantages.

 DOI: 10.5545/sv-jme.2025.1505

Table 1. Analysis methods for the static characteristics of air springs

References	Model description	Advantage	Disadvantage
Zheng et al. [18] and Chao et al. [19]	An FSI simulation model of the air spring for analyzing its vertical static stiffness	High computational accuracy	Computational inefficiency and numerical convergence challenges
Xu et al. [21]	A single-bellows CAS geometric analytical model, which assumes that the bellows profile is a single arc with a constant arc length	High computational efficiency	The assumption of a single-arc bellows profile cannot accurately describe the non-arc shapes under actual loading conditions, thereby limiting the model's applicability
Chen et al. [22]	A multi-bellows CAS geometric analytical model, which assumes that the bellows profile is a single arc with a constant arc length	The CAS geometric analytical model is extended to a multi-bellows structure	
Zheng et al. [23]	A multi-bellows CAS geometric analytical model, which assumes that the bellows profile is a single arc and accounts for the stretching deformation of the bellows	The applicability of the CAS geometric analytical model is further broadened	

In the field of research on the dynamic characteristics of air springs and vibration isolation systems, Li et al. [20] investigated the dynamic characteristics of the air spring based on the FSI simulation model and experimental study. Bester et al. [24] investigated fatigue life prediction methods of air springs through constant amplitude dynamic tests. At the theoretical research level, studies are conducted based on principles such as gas dynamics and thermodynamics. Zhu et al. [25] proposed a dynamic model of air springs that considers rubber friction and viscoelastic effects, and determined the model parameters through experiments. Luo et al. [26] established a theoretical model for predicting the vibration isolation performance of a single air spring. Zhang et al. [27] derived a theoretical model for a dual-chamber air spring system and optimized key parameters based on the model. Building on studies of air spring characteristics, the design of novel vibration isolation systems has attracted considerable research interest. Zou et al. [28] designed an air spring vibration isolation device with automatic leveling functionality. Xu et al. [29] developed a novel vibration isolation device composed of viscoelastic material, viscous fluid and air spring, which exhibits high damping characteristics. Jang et al. [30] introduced a hybrid vibration isolation system combining an air spring with a piezo-stack actuator in series. Zhang et al. [31] proposed an electromagnetic-air spring vibration isolation system, established a dynamic model, and presented methods to enhance the system's vibration isolation performance.

Observation of the actual bellows profile reveals that when the air spring is subjected to vertical loads, the bellows profile does not form a perfect arc. To address this issue, a more universally applicable double-arc extensible geometric analytical model is proposed based on the existing theoretical framework. This model decomposes the bellows profile into two segments of arcs and takes into account the effects of bellows stretching deformation. Key geometric parameters determining the double circular arc profile are identified based on the static experimental results of the CAS load-displacement relationship. Subsequently, it derives the internal pressure and other geometric parameters of the CAS when at equilibrium under specific loading conditions. Compared with the single-arc model, the double-arc model proposed in this paper can describe a wider range of profile geometries and more closely approximates the non-arc profile characteristics of the bellows under actual working conditions.

To improve the efficiency of the FSI simulation in analyzing the vibration isolation performance of CAS, a hybrid analysis method that combines the CAS geometric analytical method with FSI simulation is proposed. This method replaces the computationally expensive FSI static analysis with the geometric analytical method. Based on the geometric parameters and internal pressure of the CAS at equilibrium, derived from the proposed double-arc model, an FSI simulation model of the CAS is constructed in Fluent software to analyze its static and dynamic characteristics. By comparing the analysis results with experimental data and full-process FSI simulation results, the feasibility of the proposed double-arc model and analysis method is validated.

Finally, using the proposed hybrid analysis method, an FSI simulation model of the air spring vibration isolation system is constructed in Fluent to analyze the dynamic response. The analysis results are then compared with the full-process FSI simulation results to evaluate the accuracy and efficiency of the proposed hybrid analysis method.

2 METHODS AND MATERIALS

Fig. 1 shows the structure model of the CAS with a single bellows. The air spring is composed of two metal cover plates with cushioning blocks and a rubber bellows. The dimensional symbols of the air spring are also shown in Fig. 1.

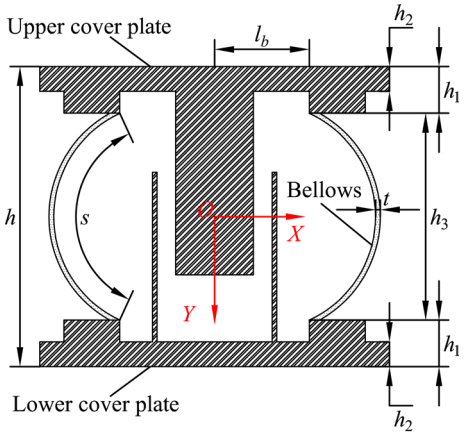

Fig. 1. The model of the CAS

2.1 The Classical Geometric Analytical Model of a CAS

Based on the research findings [21-23], the classical model of a CAS assumed a single-arc profile for the bellows, as illustrated in Fig. 2.

Some researchers [21,22] assumed a constant arc length s, while Zheng et al. [23] accounted for the stretching deformation of the bellows under working conditions. In the classical model, the corresponding central angle of the bellows arc may exceed 180° under static loading conditions. The improved model presented in Section 2.2 is proposed based on the aforementioned studies.

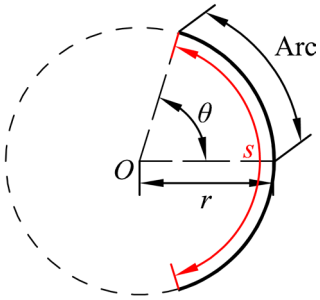

Fig. 2. The single-arc profile of the bellows

2.2 The Improved Geometric Analytical Model of a CAS

Based on the structural characteristics of the air spring, it is assumed that the profile of the bellows is changed from the traditional single arc to a shape composed of two segments of arcs, as shown in Fig. 3.

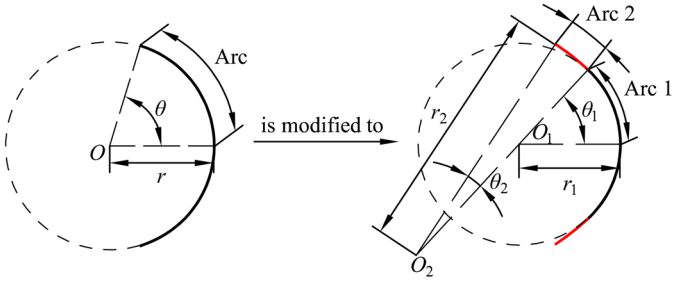

a) b)

Fig. 3. The profile of the bellows; a) single-arc profile, and b) double-arc profile

2.2.1 Volume and Internal Pressure Analysis

In the working state, the internal gas of the air spring satisfies:

$$P = P_0\left(\frac{V_{s0}}{V_s}\right)^m, \tag{1}$$

where, P is the absolute pressure, V_s is the effective volume, the subscript 0 indicates that the air spring is at its initial working height h_0. Variable m is the polytropic coefficient. The range of m is from 1 to 1.4. For an isothermal process, m=1, while for an adiabatic process, m=1.4. In the derivation of static stiffness presented in this paper, the value of m is 1.

The coordinate matrix of the centers of arc 1 and arc 2 can be expressed as:

$$\begin{bmatrix} X_{O1} & Y_{O1} \\ X_{O2} & Y_{O2} \end{bmatrix} = \begin{bmatrix} l_b - r_2\cos(\theta_1+\theta_2) + (r_2-r_1)\cos\theta_1 & 0 \\ l_b - r_2\cos(\theta_1+\theta_2) & (r_1-r_2)\sin\theta_1 \end{bmatrix}, \tag{2}$$

where, l_b is the radius of the bellows mouth, θ_1 and r_1 represent the angle and radius of arc 1, respectively. θ_2 and r_2 represent the angle and radius of arc 2, respectively.

The equation corresponding to the circle of arc i is given by:

$$(x_i - X_{Oi})^2 + (y_i - Y_{Oi})^2 = r_i^2, \quad i = 1,2. \tag{3}$$

Eq. (3) can be rewritten as:

$$x_i = X_{Oi} + \sqrt{r_i^2 - (y_i - Y_{Oi})^2}, \quad i = 1,2. \tag{4}$$

Thus, the volume of the bellows formed by the segment of arc i is:

$$V_i = 2\int_{y_{i,\min}}^{y_{i,\max}} \pi x_i^2 dy_i, \quad i = 1,2, \tag{5}$$

where,

$$\begin{cases} y_{1,\min} = 0, & y_{1,\max} = r_1\sin\theta_1 \\ y_{2,\min} = r_1\sin\theta_1, & y_{2,\max} = r_2\sin(\theta_1+\theta_2) + (r_1-r_2)\sin\theta_1 \end{cases}. \tag{6}$$

The volume of the bellows' cylindrical part can be expressed as:

$$V_b = 2A_b(h_1 - h_2), \tag{7}$$

where, h_1 is the thickness of the cover plate at the connection point between the bellows and the cover plate, h_2 is the thickness of the cover plate at its edge and A_b is given by $A_b = \pi l_b^2$.

The effective volume of the air spring V_s is equal to the sum of the volumes of the bellows' arc segment part V_a and the cylindrical part V_b, minus the volume of the cushioning blocks V_r. This can be represented as:

$$V_s = V_a + V_b - V_r = V_1 + V_2 + V_b - V_r. \tag{8}$$

Based on Eqs. (1) to (8), it is clear that the absolute pressure P is a function of the arc angle θ_1, θ_2 and the arc radius r_1, r_2.

2.2.2 Force Analysis

As shown in Figs. 4 and 5, taking the upper cover plate and the bellows as the research objects, the force balance relationship can be expressed as follows:

$$\begin{bmatrix} F+G \\ 0 \end{bmatrix} + T\begin{bmatrix} \cos(\theta_1+\theta_2) \\ 2\sin(\theta_1+\theta_2) \end{bmatrix} = (P - P_{atm})\begin{bmatrix} A_b \\ 2\pi l_b h_3 \end{bmatrix}, \tag{9}$$

where, F is the external force acting on the air spring, G is the weight of the upper cover plate, T is the tensile force of the bellows, P_{atm} is the standard atmospheric pressure and h_3 is the height of the bellows. Variable h_3 can be expressed as a function of the radii and angles of arc 1 and arc 2, that is:

$$h_3 = 2r_2\sin(\theta_1+\theta_2) - 2(r_2 - r_1)\sin\theta_1. \tag{10}$$

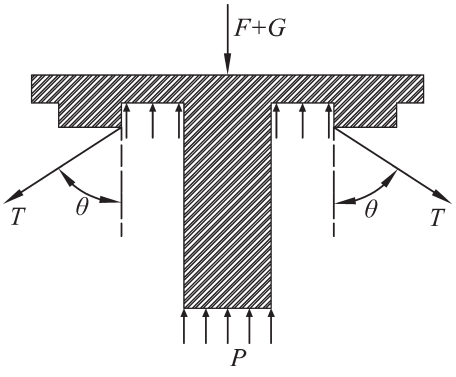

Fig. 4. Force analysis for the upper cover plate

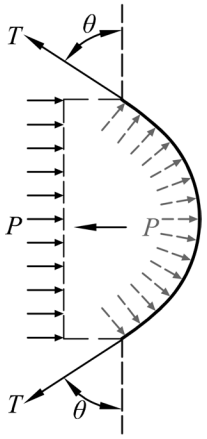

Fig. 5. Force analysis for the bellows

From Eq. (9), the following expression for F can be derived as:

$$F + G = A_e(P - P_{atm}). \tag{11}$$

where, the effective area A_e is given by $A_e=\pi l_b^2 - \pi l_b h_3 \cot(\theta_1+\theta_2)$. According to Eq. (11), the external force F is also a function of the arc angle θ_1, θ_2 and the arc radius r_1, r_2.

2.2.3 Arc Length Analysis

For the arc 1 segment within the angular range of 0 to θ'_1, and the arc 2 segment within the angular range of 0 to θ'_2, the force balance in the horizontal direction can be expressed as:

$$2\pi(P - P_{atm})\begin{bmatrix} (X_{O1} + r_1\cos\theta'_1)r_1\sin\theta'_1 \\ [X_{O2} + r_2\cos(\theta_1+\theta'_2)][r_2\sin(\theta_1+\theta'_2) + Y_{O2}] \end{bmatrix} = \begin{bmatrix} T(\theta'_1) & 0 \\ 0 & T(\theta'_2) \end{bmatrix}\begin{bmatrix} \sin\theta'_1 \\ \sin(\theta_1+\theta'_2) \end{bmatrix}. \tag{12}$$

The cross-sectional area of the bellows at angles θ'_1 and θ'_2 can be expressed as:

$$\begin{bmatrix} A(\theta'_1) \\ A(\theta'_2) \end{bmatrix} = 2\pi t\begin{bmatrix} X_{O1} + r_1\cos\theta'_1 \\ X_{O2} + r_2\cos(\theta_1+\theta'_2) \end{bmatrix}. \tag{13}$$

The increase in the length of arc i in the bellows can be represented as:

$$\Delta s_i = 2\int_0^{\theta_i} \frac{T(\theta'_i)r_i d\theta'_i}{EA(\theta'_i)}, \quad i = 1,2. \tag{14}$$

Obviously, the arc length of the bellows under working is as follows:

$$s = s_0 + \Delta s_1 + \Delta s_2, \tag{15}$$

where, s_0 is the initial arc length of the bellows when it is uninflated. The arc length s is a function of the arc angle θ_1, θ_2 and the arc radius r_1, r_2.

2.2.4 Solution via Simultaneous Equations

Based on the geometric relationship of the air spring, the following equations can be easily obtained:

$$\begin{cases} s = 2r_1\theta_1 + 2r_2\theta_2 \\ 2h_1 + h_3 = h_0 + x \\ r_2 = \alpha r_1 \\ r_2\theta_2 = \beta r_1\theta_1 \end{cases}, \tag{16}$$

where, x is the change in height of the air spring relative to the initial working height, the external profile of the bellows is controlled by parameters α and β. When the parameter $\alpha=1$ or $\beta=0$, the external profile of the bellows is a single arc. In other cases, the profile is a double circular arc. The values of α and β can be identified from the experimental results.

Obviously, in Eq. (16), h_1, h_0, and x are known data, s and h_3 are functions of the arc angle θ_1, θ_2 and the arc radius r_1, r_2. Based on Eq. (16), the values of θ_1, θ_2, r_1, and r_2 can be determined. Furthermore, by substituting the values of θ_1, θ_2, r_1, and r_2 into Eq. (11), the value of the external force F can be obtained. The vertical static stiffness of the air spring is:

$$k = \left|\frac{dF}{dx}\right|. \tag{17}$$

2.3 The Improved Hybrid Analysis Method for CAS FSI Simulation

Traditionally, performance analysis of CAS relies on a full-process FSI simulation, with its analysis process illustrated in Fig. 6. This method requires an FSI static analysis of the CAS to determine its equilibrium state under working conditions, followed by the subsequent FSI simulation. The FSI static analysis is often associated with computational inefficiency, which increases the total analysis time.

To enhance the efficiency of the traditional analysis method, an improved hybrid analysis method is proposed, with its analysis process illustrated in Fig. 7. This method replaces the computationally expensive FSI static analysis with the double-arc geometric analytical method described in Section 2.2.

The improved hybrid analysis process shown in Fig. 7 is referred to as Process I, and the traditional analysis process shown in Fig. 6 is referred to as Process II.

2.4 Experimental Study on the Characteristics of CAS

This study takes the single-bellows CAS (MKB-0390) produced by MEIRITZ SEIKI (Japan) as the research object. Table 2 shows the geometric parameters of the CAS.

Table 2. The geometric parameters of the CAS

Symbol	Unit	Value	Symbol	Unit	Value
l_b	mm	61	h_2	mm	16
h_0	mm	193	G	N	104.3
h_1	mm	30	s_0	mm	151

As shown in Fig. 8, the research team utilizes the LFV-50HH fatigue testing machine to assess the static and dynamic characteristics of the air spring, with initial pressure conditions set at 0.5 MPa and 0.7 MPa for analysis [32]. The experiments focus on investigating the dynamic characteristics of the CAS within the low-frequency range.

During the static testing phase, the specimen is vertically fixed using fixtures, and the axial load is applied in stages until the rated stroke is reached. Load-displacement data are recorded simultaneously using the built-in sensors of the testing machine. This

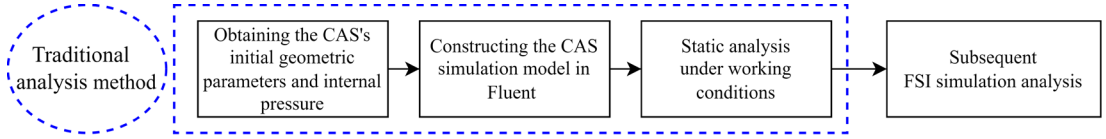

Fig. 6. The traditional analysis process of the CAS

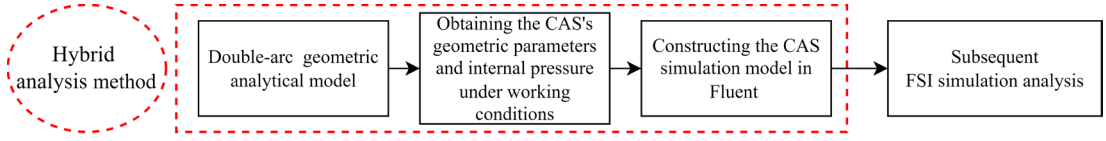

Fig. 7. The improved hybrid analysis process of the CAS

study investigates the static characteristics of the air spring under different initial pressure conditions.

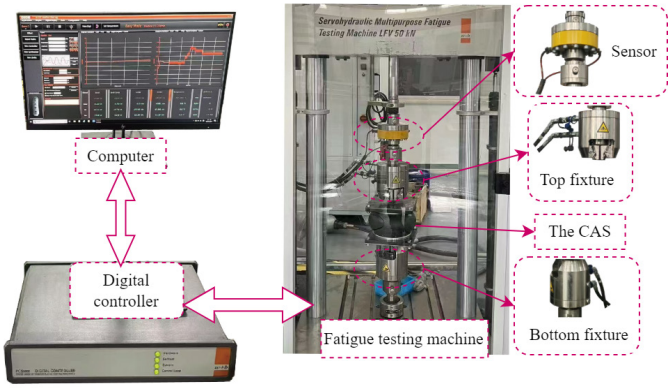

Fig. 8. Diagram of the experimental setup

The dynamic testing consists of two stages: preloading and applying excitation. First, a preload is applied to compress the air spring to the rated working height of 155 mm. Subsequently, sinusoidal excitations with a frequency interval of 1 Hz, ranging from 1 to 10 Hz, and an amplitude of 2 mm are applied to the air spring. Each frequency point is maintained for 10 cycles, and the compression and load data of the air spring are recorded under different frequency excitations. This is conducted to investigate the dynamic characteristics of the air spring under different initial pressure conditions.

Figure 9 shows the load-displacement static experimental fitting curves of the air spring at initial pressures of 0.5 MPa and 0.7 MPa. Both curves are obtained by fitting the collected data with third-order polynomials constrained to have zero intercepts.

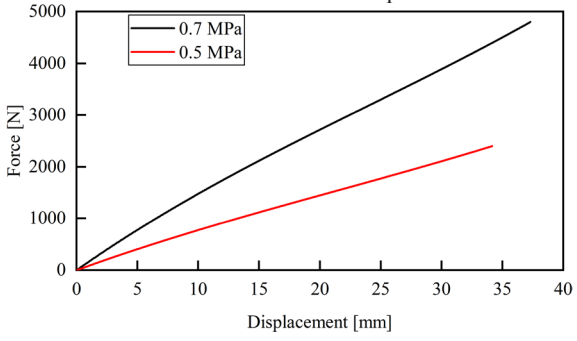

Fig. 9. Static experimental curve of the CAS

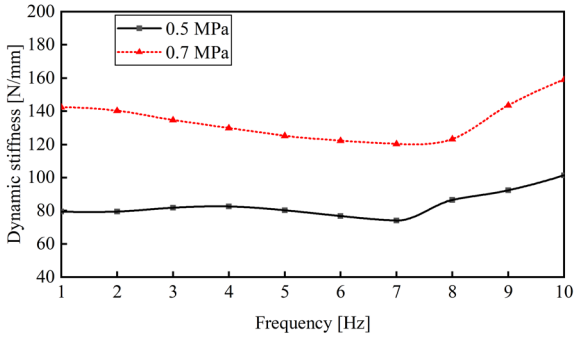

Fig. 10. Dynamic stiffness experimental data of the CAS

As shown in Fig. 9, the load-displacement curve of the CAS is basically linear. When the initial pressure increases from 0.5 MPa to 0.7 MPa, the slope of the load-displacement curve increases significantly, indicating that the initial pressure greatly influences the vertical static stiffness of the CAS. Therefore, increasing the initial pressure is an effective approach for enhancing the vertical static stiffness and load-bearing capacity. These findings demonstrate that the CAS has good stiffness adjustability, which allows it to adapt to different vibration isolation requirements.

Figure 10 presents the experimental data of dynamic stiffness for the air spring with initial air pressures of 0.5 MPa and 0.7 MPa, respectively [32]. Within the frequency range of 1 to 10 Hz, the difference between the maximum and minimum dynamic stiffness is 36.8 % at 0.5 MPa and 32.2 % at 0.7 MPa. The dynamic characteristics of the CAS are significantly influenced by the excitation frequency, showing strong frequency dependency. Like the vertical static stiffness, the dynamic stiffness of the CAS also increases with the initial pressure.

2.5 Experimental Study on the Air Spring Vibration Isolation System

To investigate the vibration transmission characteristics of the air spring vibration isolation system under excitations at different frequencies, the research team constructed an experimental setup [32]. The experimental setup primarily consists of four CAS, steel spring supports, a lower platform, an upper platform, and an XLMS electric modal exciter, as shown in Fig. 11. The initial internal pressure of the CAS is set to 0.5 MPa, with a working height of 155 mm.

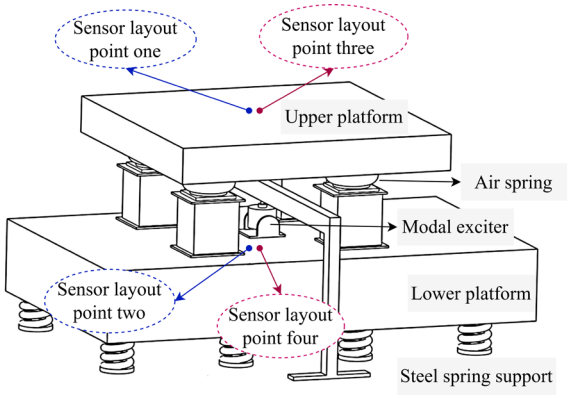

Fig. 11. Air spring vibration isolation system

When vertical excitation is applied by the exciter, four sensors are arranged at measurement points 1, 2, 3, and 4. Measurement point 2 and 4 are used to record the acceleration response of the lower platform before vibration isolation, while points 1 and 3 measure the acceleration response of the upper platform after vibration isolation. Two data acquisition systems are established for this experiment: the sensors at points 1 and 2 are connected to the XL-200 power amplifier, forming one acquisition system; the sensors at points 3 and 4 are connected to a Spider-20 dynamic analyzer for synchronized data acquisition, serving solely as a reference.

Figure 12 shows the 5 Hz and 8 Hz vertical sinusoidal excitations measured at the lower platform of the system. Figure 13 shows the acceleration response measured at the upper platform of the system after vibration isolation.

The acceleration response results indicate that the root mean square (RMS) values of the applied 5 Hz and 8 Hz acceleration excitations are 8.45×10^{-6} m/s^2 and 6.88×10^{-6} m/s^2, respectively. After vibration isolation, the vibration of the upper platform is significantly reduced, with the RMS accelerations under the 5 Hz and 8 Hz excitations reduced to 4.07×10^{-6} m/s^2 and 2.62×10^{-6} m/s^2, respectively. This significant vibration isolation effect is primarily due to the low natural frequency (below 3 Hz) of the air spring vibration isolation

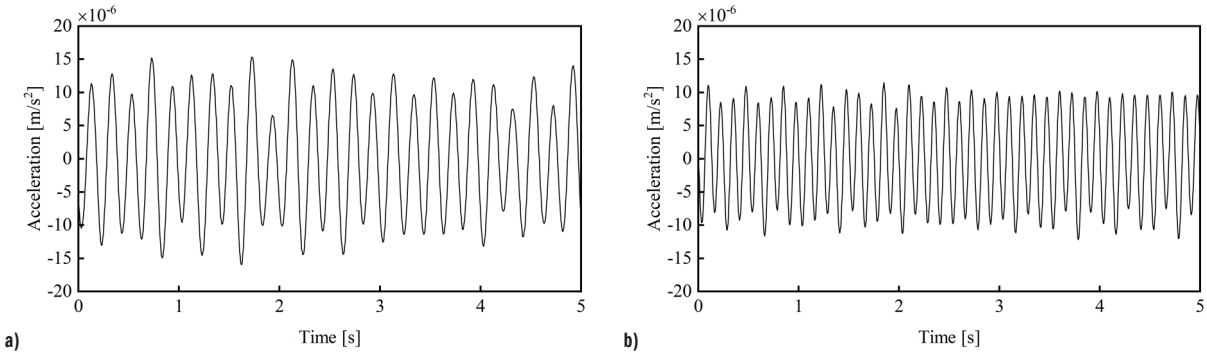

Fig. 12. The sinusoidal excitation measured at the lower platform; a) 5 Hz, and b) 8 Hz

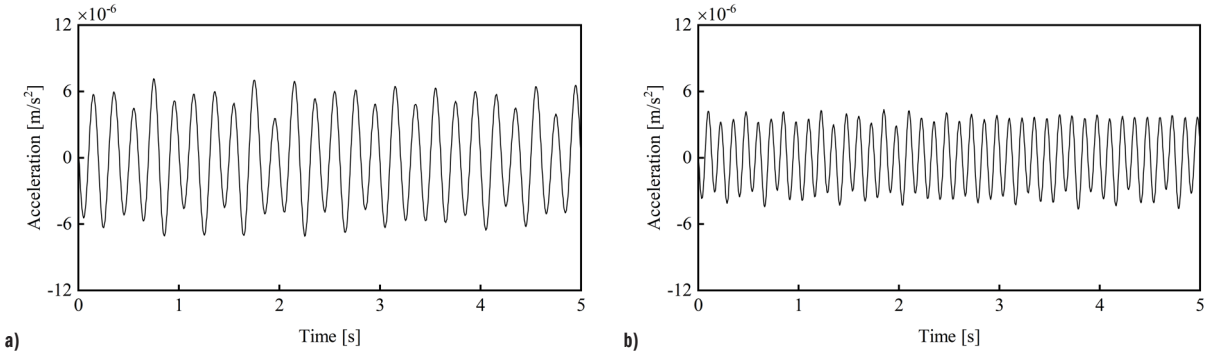

Fig. 13. The acceleration response measured at the upper platform; a) 5 Hz, and b) 8 Hz

system [32]. Notably, the vibration isolation performance under the 8 Hz excitation is superior to that under the 5 Hz excitation, which is consistent with vibration transmission theory of a single-degree-of-freedom vibration isolation system. Specifically, when the excitation frequency is greater than $\sqrt{2}$ times the system's natural frequency, the vibration isolation effect improves with the excitation frequency increase. This principle can be applied to the design of other low-frequency vibration isolation systems, but attention should be paid to the influence of load on natural frequency and damping ratio.

2.6 Numerical Simulation of the Static Characteristics

Parameter α, the radius ratio of the two arcs, is a key geometric parameter that determines the shape of the double-arc profile. Its value is based on observation of the actual geometry of the bellows under vertical load. When the air spring bears a vertical load, the middle section of the bellows undergoes more significant radial expansion compared to the two ends. The profile at the ends, where the bellows connects to the cover plates, tends to straighten due to stretching rather than maintaining the same curvature as the middle section. To better represent this deformation characteristic, parameter α is set to a large value (α=8 in this work). This setting aims to introduce a segment with smaller curvature into the profile, enabling the model to exhibit a flatter shape than the single-arc model at the same bellows length, thereby more accurately simulating the geometric features of the bellows.

Parameter β is determined entirely from static experimental data, thereby connecting the model with experimental data. Taking the condition of 0.5 MPa as an example, five characteristic points are uniformly selected within the load range of 0 to 2400 N at intervals of 600 N to establish a parameter identification process. When the profile parameter α is determined, parameter β can be uniquely determined through fitting the experimental data. Subsequently, a polynomial fitting is employed to obtain the functional expression of

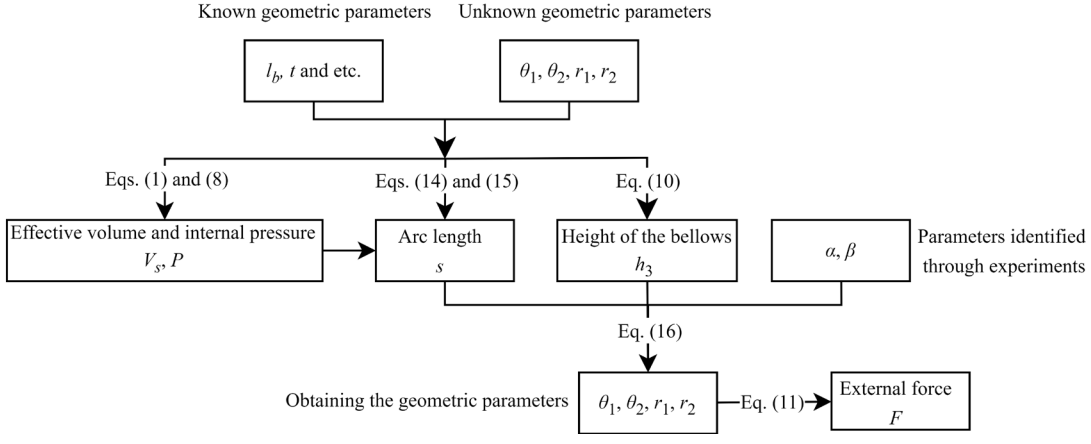

Fig. 14. The calculation process for the vertical static characteristics of the CAS

the bellows' profile parameter β as a function of the compression x. As shown in Fig. 16, when $\alpha=8$, the calculated results align well with the experimental results. The calculation process is illustrated in Fig. 14.

To further validate the applicability of the parameter selection in the double-arc model and the rationality of the hybrid analysis method proposed in this paper, two different analysis processes mentioned in Section 2.3 are employed to calculate the static and dynamic characteristics of the CAS.

Among the many factors influencing the stiffness characteristics of the CAS, the internal fluid region plays a decisive role, while factors such as the number of cord layers and their arrangement have a relatively minor influence. In this paper, the cord layers and rubber are modeled uniformly in Fluent, without establishing a separate cord layer model. The material strength of the bellows is represented by an equivalent elastic modulus of 46.5 MPa, and the air inside the model is treated as an ideal gas [32].

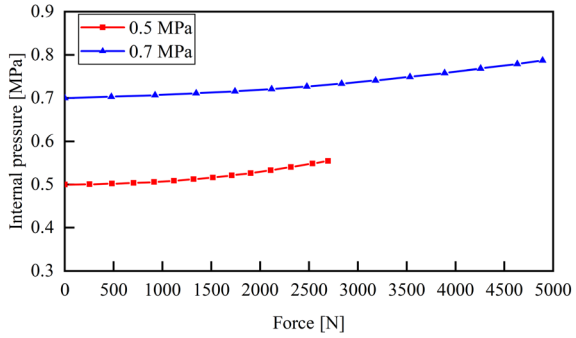

Fig. 15. The calculated internal pressure of the CAS

In the static analysis of Process I, the analysis is divided into four segments, with boundaries set at 600 N, 1200 N, and 1800 N for 0.5 MPa, and at 1200 N, 2400 N, and 3600 N for 0.7 MPa. The initial state of each segment is calculated using the geometric analytical model proposed in this study. The internal pressure calculated under different loads is shown in Fig. 15.

The data curves calculated from Process I and Process II are also shown in Fig. 16, and they show a good agreement with the experimental data.

2.7 Numerical Simulation of the Dynamic Characteristics

Figure 17 presents the dynamic stiffness calculation results from different analysis processes, along with experimental data, for initial air pressures of 0.5 MPa and 0.7 MPa in the air spring. Figure 17 demonstrates a good agreement between the dynamic stiffness obtained from different analysis processes and the experimental data. Under the 0.5 MPa condition, the maximum relative errors in dynamic stiffness between Process I and Process II, and between Process I and the experimental results, are 8.92 % and 7.68 %, respectively. Under the 0.7 MPa condition, the maximum relative errors in dynamic stiffness between Process I and Process II, and between Process I and the experimental results, are 3.74 % and 12.22 %, respectively.

2.8 Model Error Analysis and Applicability Discussion

Although Figs. 16 and 17 show good agreement between Process I, Process II, and the experimental results, noticeable errors remain. These errors are mainly caused by the model's geometric assumption and the numerical simulation:

First, the core assumption of the double-arc model proposed in this paper is that the bellows profile always consists of two arcs. Although this model can describe a wider range of profile shapes compared to the single-arc model, the actual profile during deformation may deviate from the double-arc geometry. Additionally, when calculating the stretching deformation of the bellows, the model assumes a linear elastic material and does not account for the nonlinear characteristics of the rubber and cord layers. These simplifications in both profile geometry and material model introduce unavoidable computational errors.

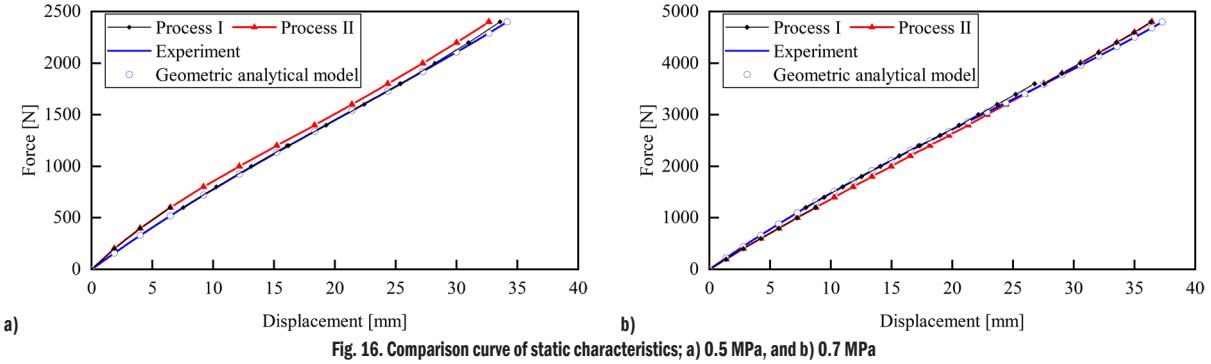

Fig. 16. Comparison curve of static characteristics; a) 0.5 MPa, and b) 0.7 MPa

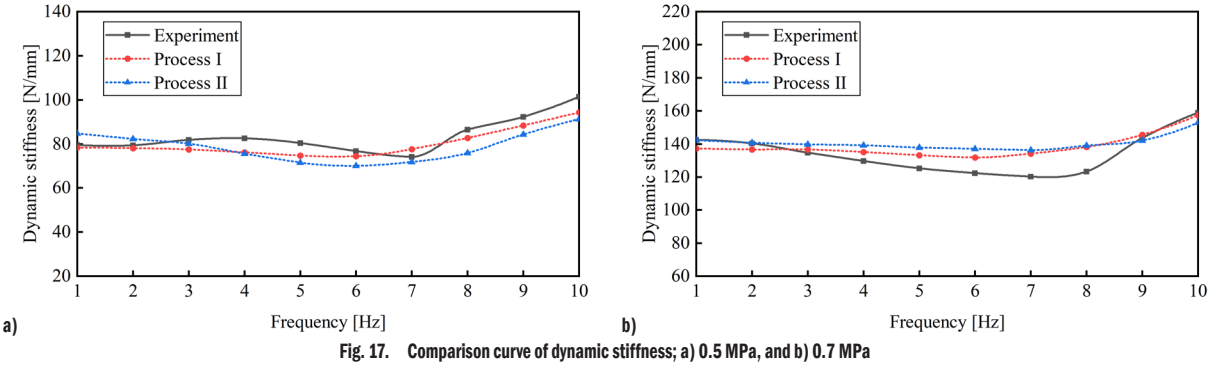

Fig. 17. Comparison curve of dynamic stiffness; a) 0.5 MPa, and b) 0.7 MPa

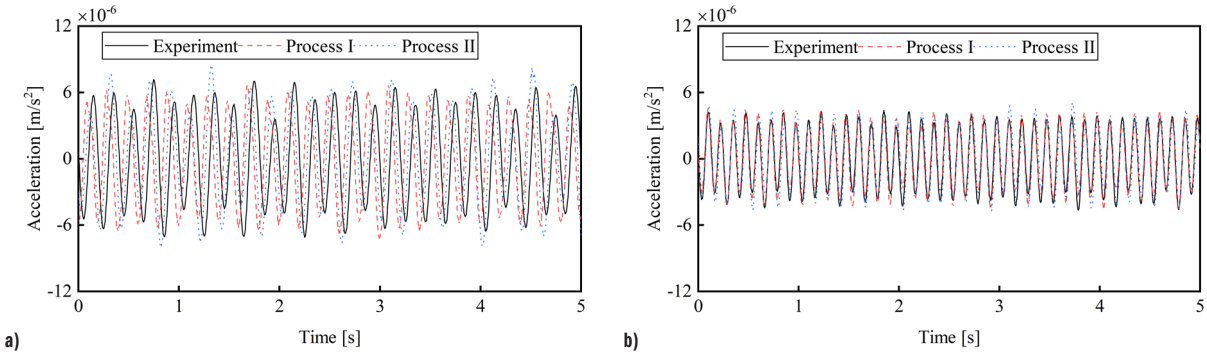

Fig. 18. Comparison curve of acceleration; a) 5 Hz, and b) 8 Hz

Second, Process I adopts a combined approach, combining the geometric analytical model with FSI simulation. The computational errors from the geometric analytical model are passed to Fluent as initial conditions and may be further amplified during subsequent simulations. Although Process II employs a full-process FSI simulation, differences remain between its simulation model and the actual air spring, such as in material parameters, leading to errors between the simulation and experimental results.

Despite being validated only at specific pressures, the model is extendable to higher pressure ranges. Geometrically, the double-arc model can effectively describe the continuous variation of the bellows profile with increasing pressure. Physically, Eq. (14) governing the stretching deformation of the bellows incorporates pressure P as a variable, ensuring theoretical self-consistency under varying pressures. Therefore, the model can demonstrate good applicability for CAS within the conventional design pressure range. However, under extreme high-pressure conditions approaching the material's limit, the model's accuracy may be affected by significant material nonlinearity not currently accounted for. Further validation and refinement using more accurate constitutive relationships are required.

3 RESULTS AND DISCUSSION

3.1 Validation of Vibration Response for Air Spring Vibration Isolation System

In this paper, an FSI simulation model of the air spring vibration isolation system is constructed in Fluent. Vertical sinusoidal excitations of 5 Hz and 8 Hz, as shown in Fig. 12, are applied to the lower platform of the model. Two different analysis processes mentioned in Section 2.3 are employed to calculate the vertical acceleration response at the same position on the upper platform of the system under excitation.

The computed results are compared with the experimental results, as shown in Fig. 18. The differences between the results obtained from the two analysis processes and the experimental test results are analyzed. The RMS value of the platform's acceleration response after vibration isolation is defined as $a_{rms,a}$, and the RMS value of the velocity response is defined as $v_{rms,a}$. Under sine excitation at 5 Hz and 8 Hz, the minor difference is observed between the results obtained from two analysis processes and experimental data. Under sine excitation at 5 Hz, the relative errors in $a_{rms,a}$ between Process I and Process II, and between Process I and the experimental result, are 4.65 % and 0.74 %, respectively. Under sine excitation at 8 Hz, the relative errors in $a_{rms,a}$ between Process I and Process II, and between Process I and the experimental result, are 4.01 % and 0.38 %, respectively. For details, refer to Table 3.

Table 3. The vibration isolation results of the air spring vibration isolation system

Excitation frequency [Hz]	Process	$a_{rms,a}$ ($\times 10^{-6}$) [m/s^2]
5	Experiment	4.07
	Process I	4.10
	Process II	4.30
8	Experiment	2.62
	Process I	2.63
	Process II	2.74

3.2 Ambient Vibration Response of Air Spring Vibration Isolation System

To further analyze the difference of the response after vibration isolation calculated by the two analysis processes, the vertical external excitation simulating ambient vibration [32], as shown in Fig. 19, is applied to the lower platform of the air spring vibration isolation system FSI simulation model, considering different loads and initial internal pressures.

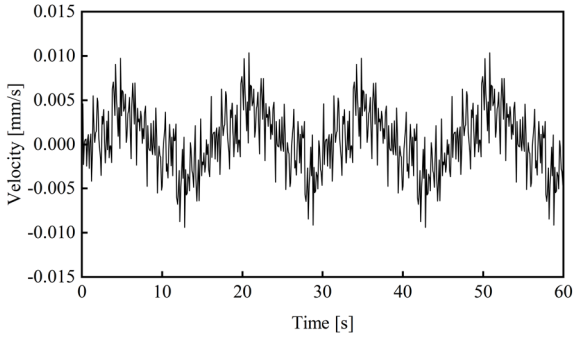

Fig. 19. External excitation

The initial air pressure of the air spring is set at 0.5 MPa, with upper loads of 2400 N, 5000 N, 7200 N, and 9600 N, respectively. The acceleration and velocity responses of the platform after vibration isolation are shown in Figs. 20 and 21, with specific results detailed in Tables 4 and 5.

When the initial air pressure of the air spring is set at 0.7 MPa, with upper loads of 4800 N, 9600 N, 14400 N, and 19200 N, the acceleration and velocity responses of the platform after vibration

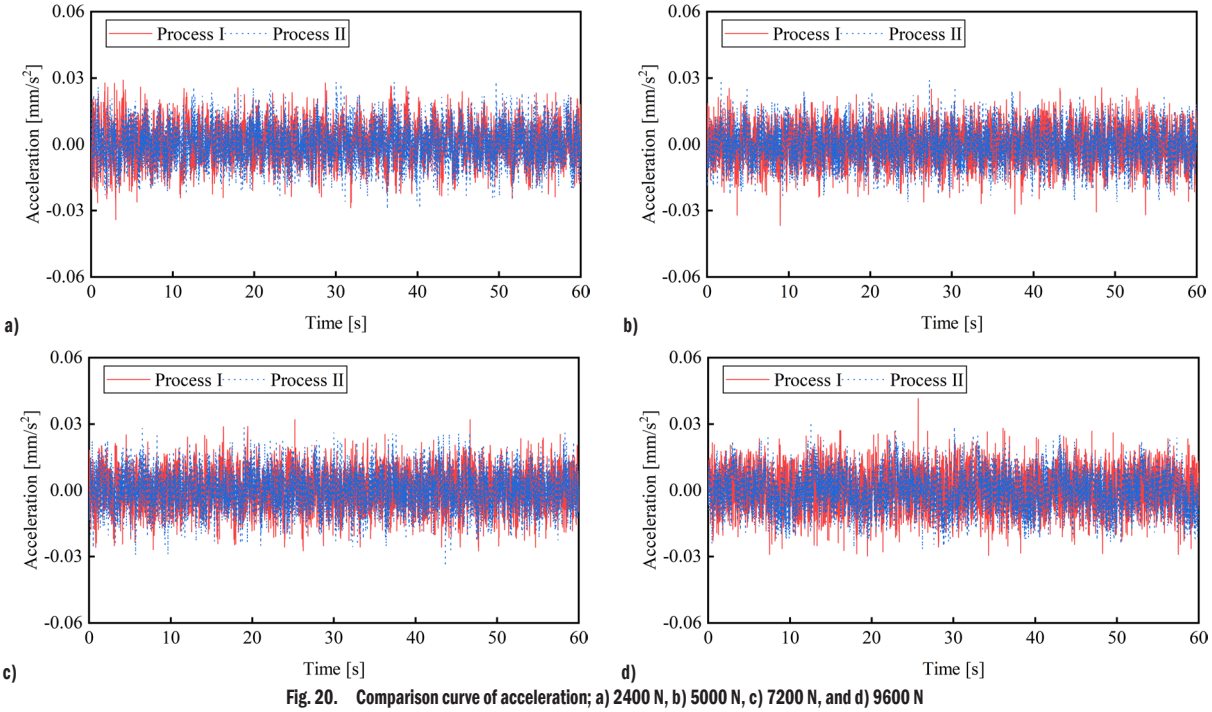

Fig. 20. Comparison curve of acceleration; a) 2400 N, b) 5000 N, c) 7200 N, and d) 9600 N

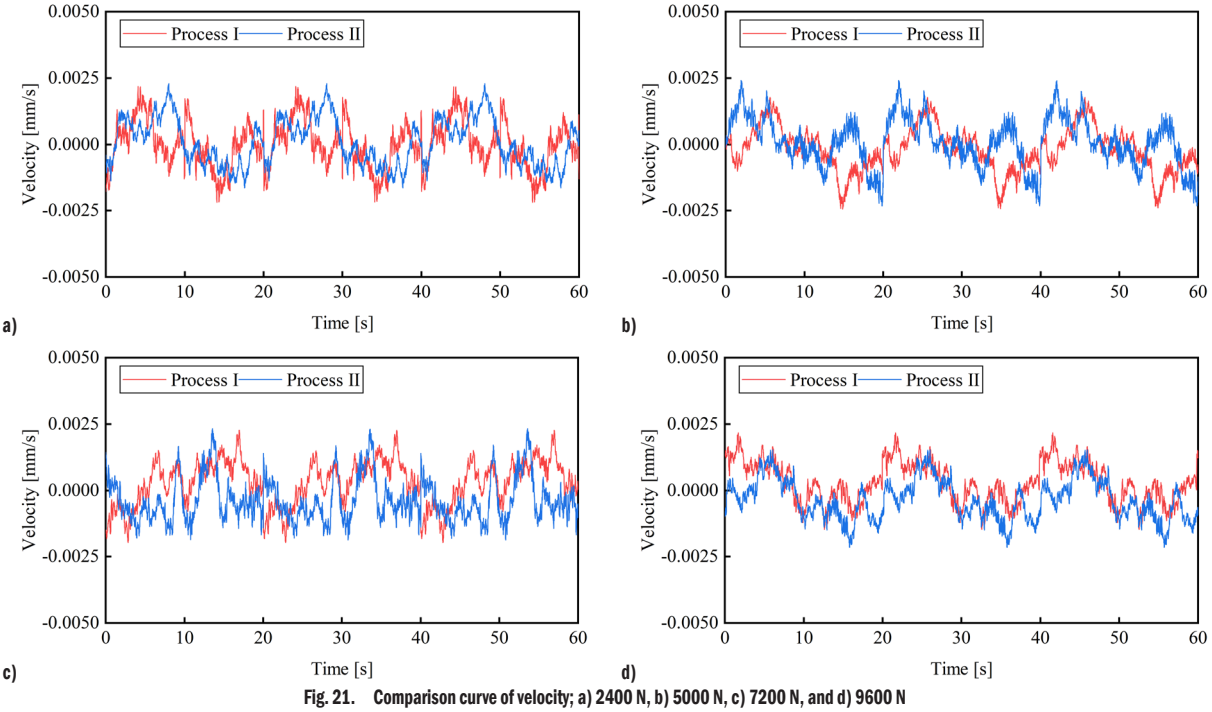

Fig. 21. Comparison curve of velocity; a) 2400 N, b) 5000 N, c) 7200 N, and d) 9600 N

isolation are shown in Figs. 22 and 23, with specific results detailed in Tables 4 and 5.

From the data presented in Tables 4 and 5, it can be observed that under different initial pressure and upper loading conditions, the maximum relative error between the RMS acceleration values obtained from Process I and Process II is 5.35 %, indicating good consistency between the two processes. The relative errors between the RMS velocity values obtained from the two processes are relatively large in two conditions, reaching 20.32% and 15.37%, respectively. In all other conditions, the errors remain below 6.47%.

With the same computational resources, the computational efficiency of Process I is superior to that of Process II. The average computational time for Process I is 24.20 hours, while for Process II, it is 27.15 hours, resulting in an average reduction of computational time by 2.95 hours, corresponding to an efficiency improvement of approximately 10.8%.

This improvement in efficiency is attributed to the replacement of the computationally expensive FSI static analysis with the geometric analytical method proposed in this study. Compared to traditional full-process FSI simulation, the proposed hybrid analysis method reduces computation time without compromising accuracy.

Notably, as the dynamic simulation time dominates the overall process, the improvement in static analysis efficiency is not significant in the overall workflow.

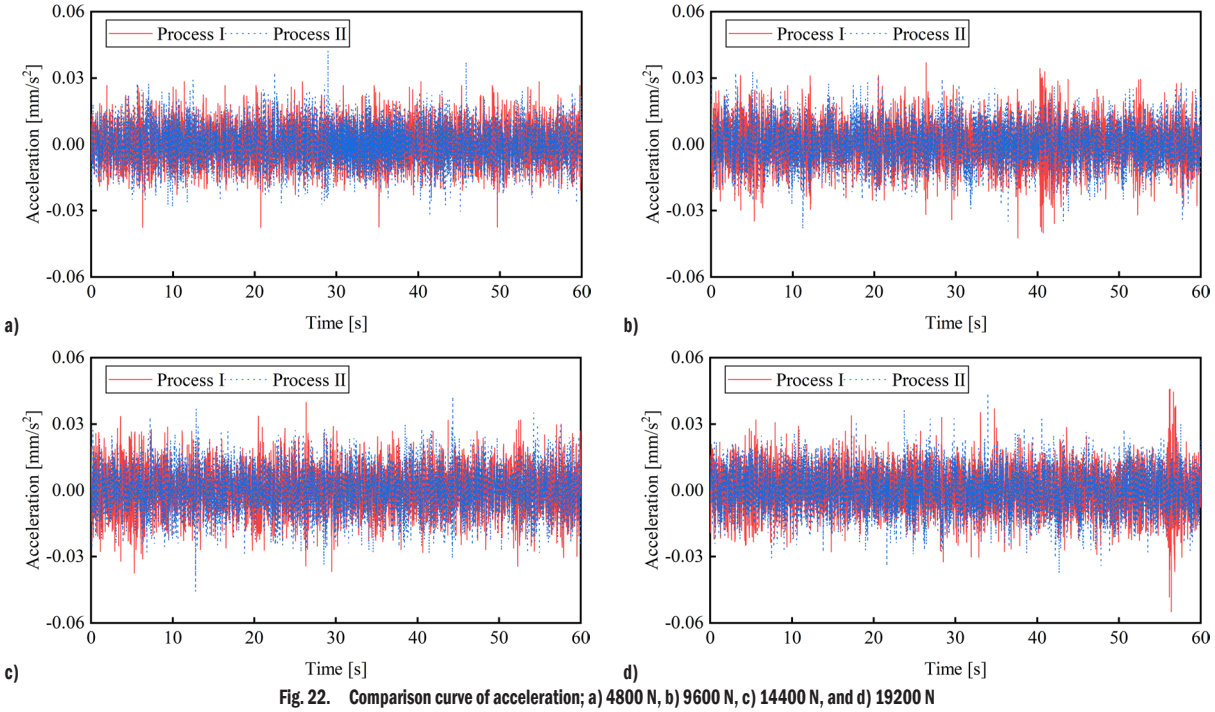

Fig. 22. Comparison curve of acceleration; a) 4800 N, b) 9600 N, c) 14400 N, and d) 19200 N

Table 4. The vibration isolation results of the air spring vibration isolation system (acceleration)

Initial pressure [MPa]	Upper load [kN]	Process	$a_{rms,a}$ [mm/s^2]
0.5	2.4	Process I	0.00852
		Process II	0.00828
	5.0	Process I	0.00794
		Process II	0.00796
	7.2	Process I	0.00841
		Process II	0.00837
	9.6	Process I	0.00886
		Process II	0.00841
0.7	4.8	Process I	0.00842
		Process II	0.00859
	9.6	Process I	0.00915
		Process II	0.00889
	14.4	Process I	0.00931
		Process II	0.00945
	19.2	Process I	0.00916
		Process II	0.00932

Table 5. The vibration isolation results of the air spring vibration isolation system (velocity)

Initial pressure [MPa]	Upper load [kN]	Process	$v_{rms,a}$ [mm/s]
0.5	2.4	Process I	0.000886
		Process II	0.000892
	5.0	Process I	0.000854
		Process II	0.000913
	7.2	Process I	0.000889
		Process II	0.000897
	9.6	Process I	0.000823
		Process II	0.000843
0.7	4.8	Process I	0.000815
		Process II	0.000963
	9.6	Process I	0.00106
		Process II	0.000881
	14.4	Process I	0.00100
		Process II	0.00104
	19.2	Process I	0.00105
		Process II	0.00111

4 CONCLUSIONS AND FUTURE WORK

A novel double-arc geometric analytical model is established to analyze the static characteristics of CAS. This model utilizes two arcs of different curvature radii to describe the bellows profile, incorporating the influence of bellows stretching deformation. Compared with the traditional single-arc model, the double-arc model can more accurately represent the actual non-arc bellows geometry.

To improve the analysis efficiency for the vibration isolation performance of CAS using FSI simulation, a hybrid analysis method is proposed. This method replaces the FSI static analysis with the geometric analytical method. Based on the geometric parameters and internal pressure of the CAS under loaded equilibrium, derived from the proposed double-arc model, an FSI simulation model of the CAS is constructed in Fluent for subsequent static and dynamic analysis. The results obtained from the hybrid analysis method show good agreement with both experimental data and results from the full-process FSI simulation, thereby validating the feasibility of the proposed double-arc model and the hybrid analysis method.

An experimental platform for the air spring vibration isolation system is developed, and tests are conducted by applying sinusoidal excitations. The maximum relative error in the RMS acceleration response between the hybrid analysis method and experimental tests is 0.74 %. In the FSI simulation of the air spring vibration isolation system under simulated ambient vibration excitation, the maximum relative error of the RMS acceleration response between the hybrid analysis method and the full-process FSI simulation is 5.35 %, indicating a slight difference. The computational efficiency of the hybrid analysis method improves by approximately 10.8 % compared

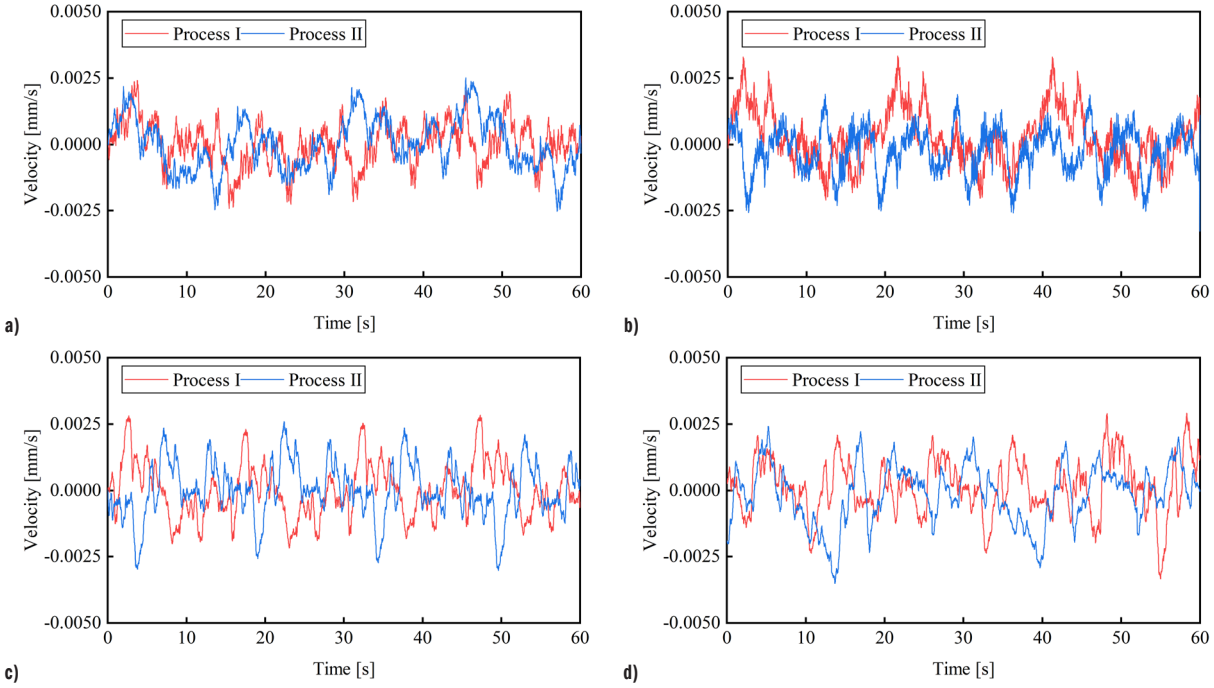

Fig. 23. Comparison curve of velocity; a) 4800 N, b) 9600 N, c) 14400 N, and d) 19200 N

to the full-process FSI simulation. The results indicate that the proposed hybrid analysis method enhances the analysis efficiency for the dynamic performance of the air spring vibration isolation system while maintaining accuracy.

It should be noted that this paper has not conducted experiments under actual random vibration conditions. Future work will involve experimental validation in actual random vibration environments to further enhance the engineering applicability of the model.

References

[1] Aralikatti, S.S., Kumar, H. Tool vibration isolation in hard turning process with magnetorheological fluid damper. *J Manuf Process* 88 (2023) 202-219 **DOI:10.1016/j.jmapro.2023.01.044**.

[2] Divijesh, P.P., Rao, M., Rao, R., Jain, N., Prabhu, P. Implementation of structurally pre-stressed piezo actuator based active vibration isolation system for micro milling. *Mater Today Proc*, 92 (2023) 182-188 **DOI:10.1016/j.matpr.2023.04.165**.

[3] Chen, S.B., Xuan, M., Xin, J., Liu, Y., Gu, S., Li, J. et al. Design and experiment of dual micro-vibration isolation system for optical satellite flywheel. *Int J Mech Sci* 179 (2020) 105592 **DOI:10.1016/j.ijmecsci.2020.105592**.

[4] Wang, C.Y., Lu, Q., Zhang, K.K., Shao, L. Design of micro-vibration suppression platform based on piezo-stack array intelligent structure. *P I Mech Eng C-J Mech* 237 (2023) 799-810, **DOI:10.1177/09544062221126624**.

[5] Ma, R.S., Bi, K.M., Hao, H. Inerter-based structural vibration control: A state-of-the-art review. *Eng Struct* 243 (2021) 112655 **DOI:10.1016/j.engstruct.2021.112655**.

[6] Liu, Y.J., Liu, J., Pan, G., Huang, Q.G. Modeling and analysis of a metal rubber vibration isolation system considering the nonlinear stiffness characteristics. *Rev Sci Instrum* 94 (2023) 015105 **DOI:10.1063/5.0118415**.

[7] Liu, Y.P., Wang, H.Y., Qiu, C.X., Zhao X.N. Seismic behavior of superelastic shape memory alloy spring in base isolation system of multi-story steel frame. *Materials* 12 (2019) 997 DOI:10.3390/ma12060997.

[8] Fu, J., Liu, G.M., Fan, C.H., Liu, Z.Y., Luo, H.T. Design and experimental study on vibration reduction of an UAV lidar using rubber material. *Actuators* 11 (2022) 345 **DOI:10.3390/act11120345**.

[9] Balaji, P.S., Rahman, M.E., Moussa, L., Lau, H.H. Wire rope isolators for vibration isolation of equipment and structures-A review. *IOP Conf Ser-Mat Sci Eng* 78 (2015) 012001 **DOI:10.1088/1757-899X/78/1/012001**.

[10] Vo, N.Y.P., Nguyen, M.K., Le, T.D. Analytical study of a pneumatic vibration isolation platform featuring adjustable stiffness *Commun Nonlinear Sci* 98 (2021) 105775 **DOI:10.1016/j.cnsns.2021.105775**.

[11] Kim, J., Lee, T., Kim, C.J., Yi, K. Development of data-based model predictive control for continuous damping and air spring suspension system. *Control Eng Pract* 142 (2024) 105777 **DOI:10.1016/j.conengprac.2023.105777**.

[12] Morales, A.L., Nieto, A.J., Chicharro, J.M., Pintado, P. A semi-active vehicle suspension based on pneumatic springs and magnetorheological dampers. *J Vib Control* 24 (2018) 808-821 **DOI:10.1177/1077546316653004**.

[13] Fang, Y., Sun, C.H., Zhu, Z.K., Zhang, G.F., Yang, H., Gao, W.W., et al. Failure analysis for air spring systems of urban rail vehicles considering load spectrum. *Eng Fail Anal* 159 (2024) 107997 **DOI:10.1016/j.engfailanal.2024.107997**.

[14] Tiwari, V., Sharma, S.C., Harsha, S.P. Ride comfort analysis of high-speed rail vehicle using laminated rubber isolator based secondary suspension. *Vehicle Syst Dyn* 61 (2023) 2689-2715 **DOI:10.1080/00423114.2022.2131584**.

[15] Qu, D., Liu, X.D., Liu, G.T., Bai, Y.F., He, T. Analysis of vibration isolation performance of parallel air spring system for precision equipment transportation. *Meas Control* 52 (2019) 291-302 **DOI:10.1177/0020294019836122**.

[16] Qu, D., Liu, X.D., Liu, G.T., He, T. Vibration isolation characteristics and control strategy of parallel air spring system for transportation under abnormal road and eccentric load conditions. *Meas Control* 54 (2021) 252-268 **DOI:10.1177/00202940211996631**.

[17] Kim, H.T., Kim, C.H., Choi, S.B., Moon, S.J., Song, W.G. A novel triple-actuating mechanism of an active air mount for vibration control of precision manufacturing machines: experimental work. *Smart Mater Struct* 23 (2014) 077003 **DOI:10.1088/0964-1726/23/7/077003**.

[18] Zheng, M., Chen, X., Lin, Y., Zhao, H. Study on nonlinear stiffness characteristics of cystiform air spring. *IEEE Vehicle Power and Propulsion Conference* (2008) **DOI:10.1109/VPPC.2008.4677469**.

[19] Chao, Y., Shen, L.M. Nonlinear stiffness characteristics and model of air spring for mattress based on finite element and numerical analysis. *Adv Theor Simul* 5 (2022) 2200393 **DOI:10.1002/adts.202200393**.

[20] Li, Y.R., Xiao, S.N., Xie, J.K., Zhu, T., Zhang, J.K. Nonlinear dynamic mechanical characteristics of air springs based on a fluid-solid coupling simulation method. *Appl Sci* 13 (2023) 12677 **DOI:10.3390/app132312677**.

[21] Xu, W., He, L., Shuai, C.G., Ye, Z.X. Stiffness calculation and dynamic simulation of air spring. *Proceedings of the ASME International Design Engineering Technical Conferences and Computers and Information in Engineering* (2005) 1395-1399 **DOI:10.1115/DETC2005-84338**.

[22] Chen, J.J., Yin, Z.H., Rakheja, S., He, J.H., Guo, K.H. Theoretical modelling and experimental analysis of the vertical stiffness of a convoluted air spring including the effect of the stiffness of the bellows. *P I Mech Eng D-J Aut* 232 (2018) 547-561 **DOI:10.1177/0954407017704589**.

[23] Zheng, Y.Q., Shangguan, W.B., Rakheja, S. Modeling and performance analysis of convoluted air springs as a function of the number of bellows. *Mech Syst Signal Pr* 159 (2021) 107858 **DOI:10.1016/j.ymssp.2021.107858**.

[24] Bester, T., Fajdiga, M., Nagode, M. Application of constant amplitude dynamic tests for life prediction of air springs at various control parameters. *Stroj Vestn-J Mech E* 60 (2014) 241-249 **DOI:10.5545/sv-jme.2013.1348**.

[25] Zhu, H.J., Yang, J., Zhang, Y.Q., Feng, X.X. A novel air spring dynamic model with pneumatic thermodynamics, effective friction and viscoelastic damping. *J Sound Vib* 408 (2017) 87-104 **DOI:10.1016/j.jsv.2017.07.015**.

[26] Luo, X.K., Li, D.X., Liu, J.Y., Zhang, H.J., Yang, X.Y. Theoretical modeling and experimental test for dynamic characteristics of an air-spring vibration isolation system. *J Braz SocMech Sci Eng* 45 (2023) 489 **DOI:10.1007/s40430-023-04389-2**.

[27] Zhang, C., Zhang, J., Feng, P., Yu, D., Wu, Z. Research on modeling and optimization of a dual chamber air spring vibration isolation system. *Adv Mater Res* 702 (2013) 310-317 **DOI:10.4028/www.scientific.net/AMR.702.310**.

[28] Zou, X.C., Li, Z.Q., Zhao, X.S., Sun, T., Zhang, K.P. Study on the auto-leveling adjustment vibration isolation system for the ultra-precision machine tool. *Proc Spie* 9281 (2014) **DOI:10.1117/12.2069463**.

[29] Xu, Z.D., Xu, Y.S., Yang, Q.Q., Xu, C., Xu, F.H., Wang, C. Tests and modeling of a new vibration isolation and suppression device. *J Dyn Syst-T ASME* 139 (2017) 121011 **DOI:10.1115/1.4036948**.

[30] Jang, D.D., Jung, H.J., Shin, Y.H., Moon, S.J., Moon, Y.J., Oh, J. Feasibility study on a hybrid mount system with air springs and piezo-stack actuators for microvibration control. *J Intel Mat Syst Str* 23 (2012) 515-526 **DOI:10.1177/1045389X11433491**.

[31] Zhang, J.G., Shu, S.Y., Song, C.S., Zhou, J., Hu, Y.F. The relationship between stiffness variation and performance of electromagnetic-air spring vibration isolator. *Adv Mech Eng* 8 (2016) **DOI:10.1177/168781401667029**.

[32] Zhang, Y.P. Study on vibration isolation performance of air-floating isolation platforms under environmental micro-vibrations and its application in semiconductor equipment, *Nanjing University of Science and Technology* (2025). (in Chinese)

Received: *2025-09-18*, **revised**: *2025-12-07, 2026-02-04*, **accepted**: *2026-02-26 as Original Scientific Paper.*

Data availability *The data that support the findings of this study are available from the corresponding author upon reasonable request.*

Author contribution *Ligang Bai: Conceptualization, Resources, Writing - original draft, Writing - review & editing; Xipeng Wang: Writing - original draft, Writing - review & editing; Hui Zhuang: Writing - review & editing; Yuanpeng Zhang: Writing - review & editing; Peng Chen: Writing - review & editing; Jianguo Ding: Writing - review & editing.*

Izboljšan model valovitih zračnih vzmeti in simulacija sistema za izolacijo vibracij z zračno vzmetjo

Povzetek *V članku je predstavljen nov analitični model z dvojno krožno krivuljo za analizo statičnih značilnosti valovitih zračnih vzmeti (CAS). Model predpostavlja, da je profil meha sestavljen iz dveh krožnih lokov z različnima polmeroma ukrivljenosti ter upošteva vpliv raztezne deformacije meha. Na osnovi tega modela je predlagana hibridna analiza, ki uporablja geometrijski analitični pristop kot nadomestilo za računsko zahtevno statično analizo interakcije med tekočino in strukturo (FSI). Z uporabo geometrijskih parametrov in notranjega tlaka v stanju obremenjenega ravnovesja določenih s predlaganim geometrijskim modelom, je bil v programu Fluent vzpostavljen FSI-simulacijski model za nadaljnjo analizo statičnih in dinamičnih značilnosti. Ustreznost modela in predlagane analitične metode je bila potrjena z eksperimentalnimi preizkusi statičnih in dinamičnih lastnosti izbrane zračne vzmeti. Nadalje je bila hibridna metoda uporabljena za analizo dinamičnega odziva sistema za izolacijo vibracij z zračno vzmetjo. Primerjava z rezultati tradicionalne celovite FSI-simulacije je pokazala, da predlagana metoda izboljša povprečno računsko učinkovitost za približno 10,8 %, ob hkratnem ohranjanju natančnosti izračunov.*

Ključne besede *valovite zračne vzmeti, statične lastnosti, dinamične lastnosti, hibridna metoda analize*